

# Automated diffeomorphic registration of anatomical structures with rigid parts: application to dynamic cervical MRI.

Olivier Commowick, Nicolas Wiest-Daesslé, Sylvain Prima

## ► To cite this version:

Olivier Commowick, Nicolas Wiest-Daesslé, Sylvain Prima. Automated diffeomorphic registration of anatomical structures with rigid parts: application to dynamic cervical MRI.. 15th International Conference on Medical Image Computing and Computer Assisted Intervention, Oct 2012, Nice, France. 15 (Pt 2), pp.163-70, 2012, LNCS. <10.1007/978-3-642-33418-4\_21>. <inserm-00716106>

**HAL Id: inserm-00716106**

**<http://www.hal.inserm.fr/inserm-00716106>**

Submitted on 10 Oct 2012

**HAL** is a multi-disciplinary open access archive for the deposit and dissemination of scientific research documents, whether they are published or not. The documents may come from teaching and research institutions in France or abroad, or from public or private research centers.

L'archive ouverte pluridisciplinaire **HAL**, est destinée au dépôt et à la diffusion de documents scientifiques de niveau recherche, publiés ou non, émanant des établissements d'enseignement et de recherche français ou étrangers, des laboratoires publics ou privés.

# Automated diffeomorphic registration of anatomical structures with rigid parts: Application to dynamic cervical MRI

Olivier Commowick<sup>1</sup>, Nicolas Wiest-Daesslé<sup>2</sup>, and Sylvain Prima<sup>1</sup>

<sup>1</sup> INRIA, INSERM, VisAGeS U746 Unit/Project, F-35042 Rennes, France  
University of Rennes I-CNRS UMR 6074, F-35042 Rennes, France

<sup>2</sup> CHU, University Hospital of Rennes, F-35043 Rennes, France  
Contact: `Olivier.Commowick@inria.fr`

**Abstract.** We propose an iterative two-step method to compute a diffeomorphic non-rigid transformation between images of anatomical structures with rigid parts, without any user intervention or prior knowledge on the image intensities. First we compute spatially sparse, locally optimal rigid transformations between the two images using a new block matching strategy and an efficient numerical optimiser (BOBYQA). Then we derive a dense, regularised velocity field based on these local transformations using matrix logarithms and M-smoothing. These two steps are iterated until convergence and the final diffeomorphic transformation is defined as the exponential of the accumulated velocity field. We show our algorithm to outperform the state-of-the-art log-domain diffeomorphic demons method on dynamic cervical MRI data.

## 1 Introduction

In medical image analysis, one is often confronted with the problem of registering anatomical structures containing both hard, rigid (typically, bones) and soft, non-rigid (most other tissues) parts. Such problems are met for instance when following-up spinal cord lesions in MRI for the diagnosis of multiple sclerosis [1], or when assessing cervical injuries using dynamic/kinematic MR imaging with positional changes [2]. Many methods have been developed for both *fully* global rigid registration and *fully* local non-rigid registration separately [3], but the literature on hybrid methods, allowing for adequate registration of the structures depending on the *stiffness* of their components, is still quite sparse.

The earliest work we know of is that of Little et al. [4], who showed how to incorporate rigid structures into a deformation field, using radial basis functions; this was later improved by others to make the field invertible and even diffeomorphic [5–7]. However, these methods require the user to specify which structures are rigid, which led to the development of semi-automated methods in which rigidity can be locally favoured/enforced through a regularisation term in the criterion to be minimised [8]. This idea was later improved to allow for this term to be adaptively tuned to the structures to register, through prior segmentation of the rigid parts or design of a stiffness map (typically computed from

the image intensities; e.g. bones have high intensities in CT) [9–11]. Instead of segmenting rigid parts, it was also proposed to define several *anchors*, to which is attached an unknown polyaffine transformation, which can be subsequently estimated using a modified EM-ICP algorithm [12].

In this paper, we propose an iterative two-step method to compute a diffeomorphic non-rigid transformation between images of structures with rigid parts, without any user intervention or prior knowledge on the image intensities (to compute rigid parts or anchors). First we compute spatially sparse, locally optimal rigid transformations between the two images by adopting a new (as opposed to classical, translation-based) block matching strategy, made possible by the use of an efficient numerical optimiser (BOBYQA) (Sec. 2.1). The rationale behind this original strategy is our hope to recover both large rotations and subvoxel displacements. Then we derive a dense, regularised velocity field based on these local transformations using matrix logarithms and M-smoothing (Sec. 2.2). The floating image is then resampled and the two steps are iterated until convergence; the final diffeomorphic transformation is defined as the exponential of the accumulated velocity field. We finally compare our algorithm with the state-of-the-art log-domain diffeomorphic demons method [13] on dynamic cervical and multiple sclerosis MR images (Sec. 3).

## 2 Material and Methods

To compute a diffeomorphism  $T$  between a reference image  $I$  and a floating image  $J$ , we iterate between two steps: computation of a sparse set of locally optimal rigid transformations using block matching between  $I$  and  $J \circ T^l$  (Sec. 2.1) and computation of a dense velocity field  $\delta LT^l$  computed from these locally estimated transformations (Sec. 2.2). Given that the transformation  $T$  is initially set to the identity ( $T^0 = Id$ ), and that the initial velocity field is set to  $LT^0 = \log T^0 = 0$ , the velocity field is then updated as  $LT^{l+1} = LT^l + \delta LT^l$ . This two-step algorithm stops at the iteration  $l$  when  $\delta LT^l$  is close to 0, and the final diffeomorphism is computed as  $T = T^l = \exp(LT^l)$ . The complete algorithm is outlined in Sec. 2.3. For the sake of clarity, we detail the two steps using the simpler notations  $I$ ,  $J$  and  $\delta LT$  (Sec. 2.1 and 2.2).

### 2.1 Computing a sparse set of locally optimal rigid transformations

**Classical block matching algorithm.** In this approach, that we *do not* follow, one first defines a set of blocks in each image, before matching each block in the reference image  $I$  with the most similar block in the floating image  $J$ . Similarity is typically computed using a measure on the voxel intensities, such as the sum of squared differences or the squared correlation coefficient in monomodal problems, or the mutual information or the correlation ratio in multimodal problems. The most common approach to optimise the similarity measure (at least in medical image analysis) is to perform an exhaustive search of the block with the highest similarity in  $J$ , within a given neighbourhood of each block in  $I$ .

This strategy implicitly assumes that the local motion between the images can be well recovered by a discrete translation (i.e. defined on the discrete grid of the image). Subvoxel displacements and large rotations are thus likely to be missed. It is all the more true when registering piecewise rigid structures, because in this case there exists no single, global rigid movement, that could be corrected before non-rigid registration.

**Modified block matching algorithm.** Recent advances in nonlinear optimisation allow for testing another strategy. We first define a set of blocks in  $I$  (as in the standard strategy), and then we propose to directly compute the rigid transformation best superposing each of these blocks with  $J$ , using a similarity measure on the voxel intensities. As opposed to the standard, discrete translation-based strategy, the computation of the similarity measure for a given block in  $I$  and a given tested transformation implies resampling to build the block in  $J$ . Given that the solution space is no longer finite, this leads to a potentially much more computationally expensive algorithm.

We propose to use the recent BOBYQA algorithm [14] to implement this idea. In essence, BOBYQA is a derivative-free, trust-region method which uses successive approximations of the similarity measure by quadratic functions, whose maxima can be computed analytically. It is very similar to the classical NEWUOA algorithm except that bounds must be specified on the variables. We thus end up with a set of blockwise-estimated optimal rigid transformations between  $I$  and  $J$ . In practice, however, we do not estimate a transformation for the blocks in  $I$  having a low variance  $\sigma^2$ . The set of estimated transformations  $(R_1, \dots, R_m)$  is thus spatially sparse, due to these missing transformations, and also due to the resolution of the grid of blocks in  $I$ , which is different from that of  $J$ . In addition, we weigh each estimated transformation  $R_i$  with a weight  $w_i$  set equal to the similarity measure; here we use the squared correlation coefficient, to be insensitive to local intensity changes, thus  $0 \leq w_i \leq 1$ .

## 2.2 Estimating a dense velocity field

The set of estimated transformations  $(R_1, \dots, R_m)$  is spatially sparse, but is also noisy and likely to contain outliers (due to the noise in the images to be registered and the potential errors in local registrations). How to estimate a dense ( $n = \text{card}(I)$ ) and smooth velocity field  $\delta LT$  from  $(R_1, \dots, R_m)$ ? We propose to use the logarithms of these  $m$  transformations, defined in the space of  $4 \times 4$  real matrices  $(\mathcal{M}_4(\mathbb{R}))$  restricted to those whose last row contains only zeros, and to estimate  $n$  intermediate matrices in the same space (that we name  $\log S_1, \dots, \log S_n$  by analogy) as the minimisers of a criterion  $C$ :

$$(\log S_1, \dots, \log S_n) = \arg \min_{\log S_1, \dots, \log S_n} \left[ \sum_{i=1}^n \sum_{j \in V_i} w_j \rho(\|\log S_i - \log R_j\|^2) d(|v_i - v_j|^2) \right],$$

where:

- $\rho : \mathbb{R} \rightarrow \mathbb{R}^+$  is a robust error norm,
- $\|\cdot\|$  is the Frobenius norm in  $\mathcal{M}_4(\mathbb{R})$ , and  $|\cdot|$  is the Euclidean norm in  $\mathbb{R}^3$ ,
- $v_j$  is the coordinate of the central voxel of the block where  $R_j$  was estimated,
- $v_i$  is the coordinate of the voxel where  $S_i$  is to be computed,
- $V_i$  is a neighbourhood around the position  $v_i$ ; note that the sum over  $j \in V_i$  must read: “the sum over all the points  $v_j$  where a rigid transformation  $R_j$  was estimated, and which are inside  $V_i$ ”,
- $w_j$  is the weight defined in Sec. 2.1,
- $d(\cdot) : \mathbb{R}^3 \rightarrow \mathbb{R}^+$  is a (spatial) error norm.

It must be clear that we *do not* estimate  $S_i$  and then its logarithm; we *do* estimate  $\log S_i$  directly; we use this notation here only as a convention for the sake of simplicity. Solving this minimisation problem is known as *local M-smoothing* [15], due to the use of a robust error norm and of spatial neighbourhoods to design  $C$ ;  $C$  can be minimised using gradient descent, where each transformation can be estimated independently of the others. Using a particular adaptive, data-dependent step size leads to an easy-to-interpret update formula for each  $\log S_i$  [15]:

$$\log S_i^{k+1} = \frac{\sum_{j \in V_i} w_j \rho'(\|\log S_i^k - \log R_j\|^2) d(|v_i - v_j|^2) \log R_j}{\sum_{j \in V_i} w_j \rho'(\|\log S_i^k - \log R_j\|^2) d(|v_i - v_j|^2)}$$

It can be seen from this formula that  $\rho'$  acts as a *tonal* kernel, while  $d$  acts as a *spatial* kernel. After convergence, each finally estimated  $\log S_i$  is a linear combination of the logarithms of the rigid transformations  $R_j$ ; following Arsigny et al. [5], we define the final dense velocity field  $\delta LT$  as  $\delta LT(v_i) = \log(S_i).v_i$ ,  $\forall i = 1, \dots, n$ . In practice, we define  $\rho$  as the Welsch function, which leads to  $\rho'(a^2) = \exp(-a^2/2\lambda^2)$ , and we define  $d$  as  $d(b^2) = \exp(-b^2/2\theta^2)$ ; this leads to two similar expressions for the two kernels (with different bandwidths).  $V_i$  is spherical with radius  $2\theta$  (to achieve an approximate 95% confidence interval for a Gaussian law). To initialise the gradient descent algorithm,  $S_i^0$  is computed as the solution of the update formula by setting  $\rho'(a^2) = 1$  (i.e. no tonal kernel).

### 2.3 Complete algorithm

The final estimated transformation is a diffeomorphism [5]. We perform all the update calculations on the velocity field, whose exponential is required only once per iteration to resample the floating image. This is the same approximation as that done by Vercauteren et al., who showed experimentally that  $\exp(LT^{l-1}) \circ \exp(\delta LT)$  could be approximated by  $\exp(LT^{l-1} + \delta LT)$  for a small enough velocity field  $\delta LT$  [13].

### 2.4 Implementation details

For the **block matching**: size of the blocks: 7 voxels; grid step size: 3 voxels; minimal intensity variance in the blocks: 1/4 of the maximum squared intensity; search radiuses within BOBYQA: 2 voxels (translation) and 5 degrees (rotation).

---

**Algorithm**

---

- 1: Initialize  $T$  to identity:  $T^0 \leftarrow Id = \exp(LT^0)$  and the velocity field to 0:  $LT^0 \leftarrow 0$
  - 2: **for** each pyramid level of the multiresolution scheme, **do**
  - 3:   **repeat**
  - 4:     Estimate local rigid transformations using block matching (Sec. 2.1):  
       $R = (R_1, \dots, R_m) \leftarrow \text{block-matching}(I, J \circ T^{l-1})$
  - 5:     Interpolate a dense velocity field using M-smoothing (Sec. 2.2):  
       $\delta LT \leftarrow \text{M-smooth}(R)$
  - 6:     Increment the velocity field:  $LT^l = LT^{l-1} + \delta LT$
  - 7:     Regularise (elastic-like) the velocity field:  $LT^l \leftarrow G_\nu * LT^l$
  - 8:     Compute  $T^l = \exp(LT^l)$  to resample  $J$
  - 9:   **until**  $\delta LT$  is sufficiently small
- 

For the **M-smoothing**: kernel bandwidths:  $\lambda^2 = \text{med}_{j \neq h} \|\log R_j - \log R_h\|^2 / 2$  (tonal),  $\theta = 4$  voxels (spatial);  $\nu = 4$  voxels in the elastic-like regularisation. We use a 3-level multiresolution strategy, and the resampling of the floating image is done using trilinear interpolation. Run-time of the algorithm (dual core Xeon 3.0 GHz PC): about 6 min (vs 2 min for the log-domain diffeomorphic demons [13]).

### 3 Validation and Results

We propose to assess our algorithm quantitatively on ten patients with traumatic cervical cord injury, who got dynamic cervical MRI (T2-w, size  $384 \times 384 \times 14$ , voxel size  $0.8 \times 0.8 \times 3 \text{ mm}^3$ ) with two different positions each: either flexion/neutral, or extension/neutral [2]. For each patient, we manually defined landmarks on the cervical/thoracic vertebrae C1-C3-C6-T1 (and T4 when visible), the pontomedullary junction, and the gnathion (lower border of the mandible) on each of the two MRI. We considered the neutral position as the reference image in the extension/neutral setting, and the flexion as the reference image in the flexion/neutral setting. For a given patient, the registration accuracy was evaluated as the root mean square error (RMSE) computed over the homologous landmarks after registration using four different methods: global rigid registration ( $M_1$ ) [16], log-domain diffeomorphic demons ( $M_2$ ) [13], our algorithm ( $M_3$ ), and  $M_2$  initialised using  $M_3$  ( $M_4$ ); both  $M_2$  and  $M_3$  are initialised using  $M_1$ . We also assessed our algorithm visually on two patients with MS lesions in the spinal cord, and two other patients with tumours in the spinal cord, with two time points each (T1-w, size  $256 \times 256 \times 64$ , voxel size  $1 \times 1 \times 1 \text{ mm}^3$ ).

The box-and-whisker plot in Fig. 1 computed from the ten patients shows our algorithm ( $M_3$ ) to significantly outperform both  $M_1$  (paired t-test:  $p = 3 \times 10^{-4}$ ) and  $M_2$  (paired t-test:  $p = 2 \times 10^{-3}$ ), with much smaller error and much smaller error dispersal.  $M_3$  is also slightly better than  $M_4$  (paired t-test:  $p = 5 \times 10^{-2}$ ). This suggests that the log-domain diffeomorphic demons performs worse than our algorithm even when properly initialised (using  $M_3$  instead of  $M_1$ ). The results of  $M_1$ ,  $M_2$  and  $M_3$  on one of the ten patients are shown in Fig. 2, and that of  $M_1$  and  $M_3$  are shown on one of the MS patients in Fig. 3.

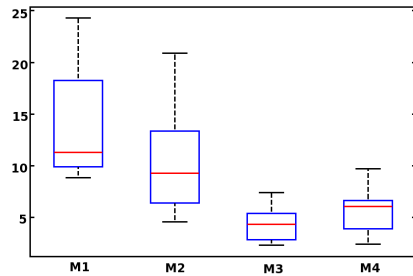


**Fig. 1. Quantitative evaluation of registration accuracy.** Box-and-whisker plot of registration errors (unit: millimetres) for the 4 compared methods ( $M_1$  to  $M_4$ ). The errors and the error dispersal are much smaller for  $M_3$  compared to  $M_1$  and  $M_2$ ;  $M_4$  is also slightly worse than  $M_3$ , which suggests that  $M_4$  actually degrades the results compared to  $M_3$  when initialised with  $M_3$ .

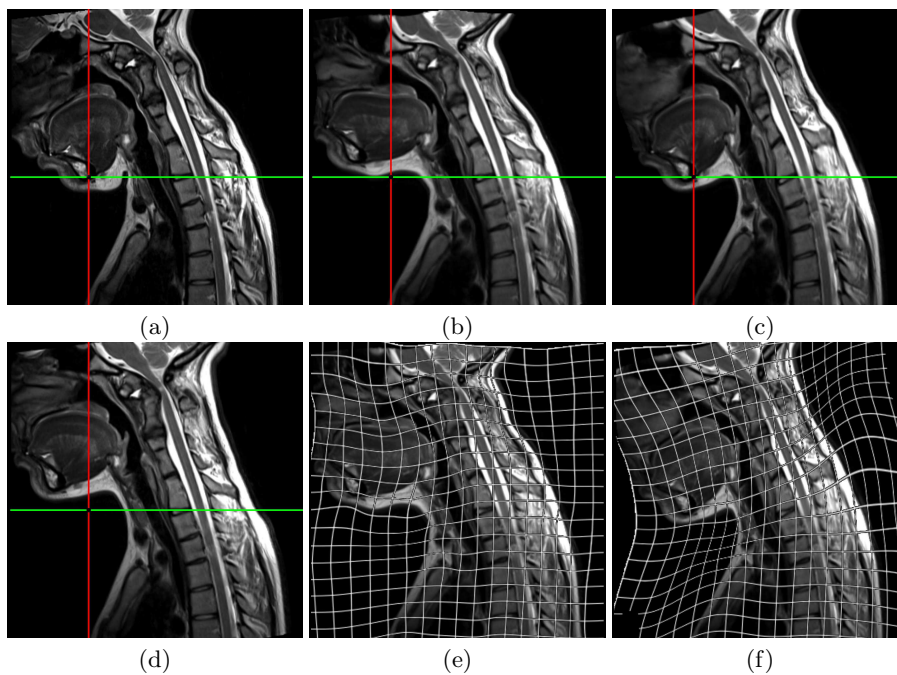


**Fig. 2. Registration results on a patient with flexion/neutral positions.** (a) reference image; (d,b,c) floating image registered to the reference image with  $M_1$ ,  $M_2$ ,  $M_3$  respectively; (e,f) same as (b,c) with deformation grids overlaid. The intersection between the green and red lines shows the large error of  $M_2$  on the mandible; on the contrary,  $M_3$  correctly matches this point. The ability of  $M_3$  to recover the flexion is further illustrated by the deformation grid: the deformation visually appears as near-rigid on the lower head and face, while it shows extension near the back of the neck and contraction near the front of the neck; on the contrary, the deformation grid shows that  $M_2$  outputs near rigid movement everywhere.

## 4 Conclusion & Perspectives

It appears that our strategy for non-rigid registration, based on the computation of locally optimal rigid transformations in the first place, allows us to recover

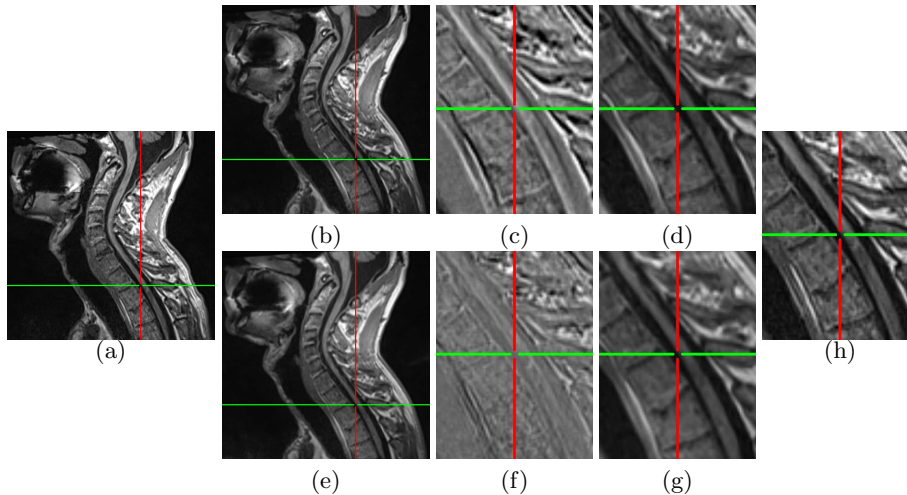


**Fig. 3. Registration results on a patient with MS lesions in the spinal cord.** (a) patient image at time point  $t_0$ ; (b) patient image at time point  $t_1$  registered with  $M_1$  and (e) with  $M_3$ ; (d,g) zoom on (b,e); (h) zoom on (a); (c,f) zoom on the difference (registered minus reference) image. Note that in this case  $M_2$  (not displayed) performs as well as  $M_3$ . These snapshots, and in particular the zoomed difference images, visually show that  $M_3$  gives a better result than a simple global rigid registration.

displacements and deformations of piecewise rigid structures (as seen e.g. in dynamic cervical MRI) much better than standard methods which are implicitly based on locally optimal translations, such as the log-domain diffeomorphic demons algorithm. This original strategy was made possible by (i) the use of an up-to-date very efficient optimiser and (ii) the design of a specific regularising procedure on the (sparse) set of locally estimated rigid transformations, based on robust estimation techniques. A future line of research could be to combine our regularisation technique with those previously proposed in this context [9–11]. Our intuition is also that our algorithm could perform very well in more general problems, without necessarily rigid structures involved, and on other image modalities; we will evaluate this in a near future.

**Acknowledgments.** We thank Élise Bannier, Jean-Yves Gauvrit and Aurore Esquevin (CHU, University Hospital of Rennes, F-35043 Rennes, France) for discussions on the clinical protocol and for acquiring the MR images. We also thank Charles Kervrann (INRIA, SERPICO Project, F-35042 Rennes, France) for last-minute and life-saving reading suggestions.

## References

1. Okuda, D., Mowry, E., Cree, B., Crabtree, E., Goodin, D., Waubant, E., Pelletier, D.: Asymptomatic spinal cord lesions predict disease progression in radiologically



- isolated syndrome. *Neurology* **76**(8) (2011) 686–692
2. Abitbol, J.J., Hong, S.W., Khan, S., Wang, J.C.: Dynamic MRI of the spine. In Szpalski, M., Gunzburg, R., Rydevik, B.L., Huec, J.C., Mayer, H.M., eds.: *Surgery for Low Back Pain*. Springer (2010) 39–45
  3. Maintz, J., Viergever, M.: A survey of medical image registration. *Med Image Anal* **2**(1) (1998) 1–36
  4. Little, J., Hill, D., Hawkes, D.: Deformations Incorporating rigid structures. *Comput Vis Image Und* **66**(2) (1997) 223–232
  5. Arsigny, V., Commowick, O., Ayache, N., Pennec, X.: A Fast and Log-Euclidean Polyaffine Framework for Locally Linear Registration. *J Math Imaging Vis* **33**(2) (2009) 222–238
  6. Commowick, O., Arsigny, V., Isambert, A., Costa, J., Dhermain, F., Bidault, F., Bondiau, P.Y., Ayache, N., Malandain, G.: An efficient locally affine framework for the smooth registration of anatomical structures. *Med Image Anal* **12**(4) (2008) 427–441
  7. Seiler, C., Pennec, X., Reyes, M.: Geometry-Aware Multiscale Image Registration via OBBTree-Based Polyaffine Log-Demons. In Fichtinger, G., Martel, A., Peters, T., eds.: *MICCAI'2011*. Vol. 6892 of LNCS, Springer (2011) 631–638
  8. Rohlfing, T., Maurer, C.: Intensity-based non-rigid registration using adaptive multilevel free-form deformation with an incompressibility constraint. In Niessen, W., Viergever, M., eds.: *MICCAI'2001*. Vol. 2208 of LNCS, Springer (2001) 111–119
  9. Loeckx, D., Maes, F., Vandermeulen, D., Suetens, P.: Nonrigid image registration using free-form deformations with a local rigidity constraint. In Barillot, C., Haynor, D., Hellier, P., eds.: *MICCAI'2004*. Vol. 3216 of LNCS, Springer (2004) 639–646
  10. Ruan, D., Fessler, J.A., Roberson, M., Balter, J., Kessler, M.: Nonrigid registration using regularization that accomodates local tissue rigidity. In Reinhardt, J.M., Pluim, J.P., eds.: *Medical Imaging 2006: Image Processing*, SPIE Press (2006)
  11. Staring, M., Klein, S., Pluim, J.P.: A rigidity penalty term for nonrigid registration. *Med Phys* **34**(11) (2007) 4098–4108
  12. Taquet, M., Macq, B., Warfield, S.: Spatially Adaptive Log-Euclidean Polyaffine Registration Based on Sparse Matches. In Fichtinger, G., Martel, A., Peters, T., eds.: *MICCAI'2011*. Vol. 6892 of LNCS, Springer (2011) 590–597
  13. Vercauteren, T., Pennec, X., Perchant, A., Ayache, N.: Symmetric log-domain diffeomorphic registration: A demons-based approach. In Metaxas, D., Axel, L., Fichtinger, G., Székely, G., eds.: *MICCAI'2008*. Vol. 5241 of LNCS, Springer (2008) 754–761
  14. Powell, M.: *The BOBYQA algorithm for bound constrained optimization without derivatives*. Technical report, Centre for Mathematical Sciences, University of Cambridge, UK (2009)
  15. Mrazek, P., Weickert, J., Bruhn, A.: On robust estimation and smoothing with spatial and tonal kernels. In Klette, R., Kozera, R., Noakes, L., Weickert, J., eds.: *Geometric Properties for Incomplete data*. Springer (2006) 335–352
  16. Ourselin, S., Roche, A., Prima, S., Ayache, N.: Block Matching: A General Framework to Improve Robustness of Rigid Registration of Medical Images. In Delp, S., DiGioia, A., Jaramaz, B., eds.: *MICCAI'2000*. Vol. 1935 of LNCS, Springer (2000) 557–566